UNIVERSITY OF BIRMINGHAM
University of Birmingham Research at Birmingham

Influence of Poly(styrene- co-maleic acid) Copolymer Structure on the Properties and Self-Assembly of SMALP Nanodiscs

Hall, Stephen C L; Tognoloni, Cecilia; Price, Gareth J; Klumperman, Bert; Edler, Karen J; Dafforn, Tim R; Arnold, Thomas

DOI:
10.1021/acs.biomac.7b01539

License:
Other (please specify with Rights Statement)

Document Version
Publisher's PDF, also known as Version of record

Citation for published version (Harvard):
Hall, SCL, Tognoloni, C, Price, GJ, Klumperman, B, Edler, KJ, Dafforn, TR & Arnold, T 2018, 'Influence of Poly(styrene- co-maleic acid) Copolymer Structure on the Properties and Self-Assembly of SMALP Nanodiscs', *Biomacromolecules*, vol. 19, no. 3, pp. 761-772. https://doi.org/10.1021/acs.biomac.7b01539

Link to publication on Research at Birmingham portal

Publisher Rights Statement:
Checked for eligibility: 16/05/2018
ACS AuthorChoice - This is an open access article published under an ACS AuthorChoice License, which permits copying and redistribution of the article or any adaptations for non-commercial purposes.

General rights
Unless a licence is specified above, all rights (including copyright and moral rights) in this document are retained by the authors and/or the copyright holders. The express permission of the copyright holder must be obtained for any use of this material other than for purposes permitted by law.

•Users may freely distribute the URL that is used to identify this publication.
•Users may download and/or print one copy of the publication from the University of Birmingham research portal for the purpose of private study or non-commercial research.
•User may use extracts from the document in line with the concept of ‘fair dealing’ under the Copyright, Designs and Patents Act 1988 (?)
•Users may not further distribute the material nor use it for the purposes of commercial gain.

Where a licence is displayed above, please note the terms and conditions of the licence govern your use of this document.

When citing, please reference the published version.

Take down policy
While the University of Birmingham exercises care and attention in making items available there are rare occasions when an item has been uploaded in error or has been deemed to be commercially or otherwise sensitive.

If you believe that this is the case for this document, please contact UBIRA@lists.bham.ac.uk providing details and we will remove access to the work immediately and investigate.

Download date: 26. Apr. 2024

This is an open access article published under an ACS AuthorChoice License, which permits copying and redistribution of the article or any adaptations for non-commercial purposes.

Article

Cite This: Biomacromolecules 2018, 19, 761−772

pubs.acs.org/Biomac

Influence of Poly(styrene-*co*-maleic acid) Copolymer Structure on the Properties and Self-Assembly of SMALP Nanodiscs

Stephen C. L. Hall,[†,‡] Cecilia Tognoloni,[§,∥] Gareth J. Price,[§] Bert Klumperman,[⊥] Karen J. Edler,[§] Tim R. Dafforn,[†] and Thomas Arnold*[,‡,#]

[†]School of Biosciences, University of Birmingham, Edgbaston, Birmingham B15 2TT, United Kingdom

[‡]Diamond Light Source, Harwell Science and Innovation Campus, Didcot OX11 ODE, United Kingdom

[§]Department of Chemistry, University of Bath, Claverton Down, Bath BA2 7AY, United Kingdom

[∥]ISIS Neutron and Muon Source, Science and Technology Facilities Council Rutherford Appleton Laboratory, Harwell, Didcot OX11 0QX, United Kingdom

[⊥]Department of Chemistry and Polymer Science, Division of Polymer Science, Stellenbosch University, De Beers Street, Stellenbosch 7600, South Africa

Supporting Information

ABSTRACT: Polymer stabilized nanodiscs are self-assembled structures composed of a polymer belt that wraps around a segment of lipid bilayer, and as such are capable of encapsulating membrane proteins directly from the cell membrane. To date, most studies on these nanodiscs have used poly(styrene-*co*-maleic acid) (SMA) with the term SMA-lipid particles (SMALPs) coined to describe them. In this study, we have determined the physical and thermodynamic properties of such nanodiscs made with two different SMA copolymers. These include a widely used and commercially available statistical poly(styrene-*co*-maleic acid) copolymer (coSMA) and a reversible addition−fragmentation chain transfer synthesized copolymer with narrow molecular weight distribution and alternating styrene and maleic acid groups with a polystyrene tail, (altSMA). We define phase diagrams for each polymer, and show that, regardless of polymer topological structure, self-assembly is driven by the free energy change associated with the polymers. We also show that nanodisc size is polymer dependent, but can be modified by varying polymer concentration. The thermal stability of each nanodisc type is similar, and both can effectively solubilize proteins from the *E. coli* membrane. These data show the potential for the development of different SMA polymers with controllable properties to produce nanodiscs that can be optimized for specific applications and will enable more optimized and widespread use of the SMA-based nanodiscs in membrane protein research.

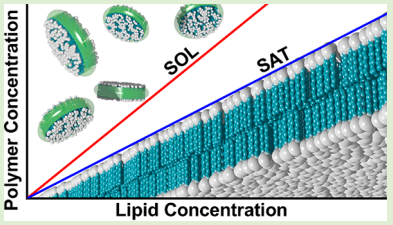

INTRODUCTION

With the ever increasing interest in biological membrane research, there is a need for appropriate model systems to study these large, multicomponent, dynamic systems without perturbing the very properties that make biological membranes so essential and fascinating. Membrane proteins represent around 30% of the proteome[1−3] and constitute >70% of therapeutic targets.[4] While knowledge of membrane proteins has been increasing,[5−7] there is still a limited amount of structural and functional information available compared to soluble proteins, largely due to their inherent insolubility and instability in aqueous media. One traditional strategy in membrane research is the use of detergents to aid solubilization. They replace the lipid annulus around the hydrophobic core to solubilize the protein inside a detergent micelle, while keeping it relatively stable so that structural and functional information can be obtained.[8,9] The principal problem with these methods is that detergents are a poor replacement for lipids.[10] Recent work has shown that the lipid annulus can have specific interactions with the membrane protein and has roles in stability and function of many transmembrane proteins.[11,12] While a detergent is amphipathic like a phospholipid, it lacks the specific chemical moieties which interact with the protein of interest.

Attempts to overcome these problems led to the development of membrane mimetic systems such as amphipols, bicelles and nanodiscs (for more information, see ref 13). Nanodiscs are self-assembled structures comprising a planar "disc" shaped segment of phospholipid bilayer which is stabilized by a surrounding protein or polymer belt. The first nanodiscs were formed by the amphipathic membrane scaffold protein (MSP) which wraps around the hydrophobic lipid tails to stabilize the nanodisc structure.[14] These MSP-nanodiscs have proven effective in membrane protein solubilization[15] and have been amenable to structural studies using a range of techniques.[16−22] However, while the protein is kept in a stable environment, the production of MSP-nanodiscs requires the protein first to be

Received: October 27, 2017
Revised: December 20, 2017
Published: December 22, 2017

© 2017 American Chemical Society

DOI: 10.1021/acs.biomac.7b01539
Biomacromolecules 2018, 19, 761−772

extracted within a detergent micelle and then reconstituted into a nanodisc.

Polymer-stabilized nanodiscs, commonly termed (SMA) lipid particles (SMALPs) use the amphipathic poly(styrene-*co*-maleic acid) SMA copolymer (Figure 1a) to wrap around the lipid tails to stabilize the lipids within a nanodisc structure. The SMA copolymer has statistically arranged styrene and maleic acid groups which are thought to self-assemble into nanodisc structures by intercalating the planar styrene rings into the lipid tails (perpendicular to the plane of the bilayer, analogous to the incorporation of cholesterol into a lipid bilayer) with the maleic acid groups allowing solubilization through hydrogen bonding and ionic interactions with the aqueous solvent.[23] SMALPs have the advantage over MSP-nanodiscs that the protein can be extracted straight from the native membrane by SMA, without having to be reconstituted into a detergent micelle thus keeping the essential lipid annulus present.[24−31] Since their discovery SMALPs have also proven to be effective in structural studies of membrane proteins utilizing techniques such as circular dichroism, analytical ultracentrifugation, electron microscopy, solid state NMR spectroscopy and X-ray crystallography.[24,32−34] SMALPs have also been shown to maintain both the structural stability and function of the encapsulated membrane proteins far more effectively than detergent alternatives.[26] Studies have also shown that the local environment within a SMALP is very similar in terms of physical properties to the native environment of the membrane proteins.[35]

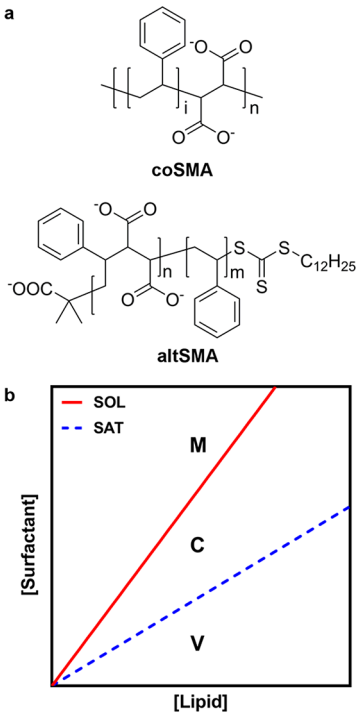

Figure 1. (a) Structures of coSMA, where on average $\langle i \rangle$ = 2, corresponding to the 2:1 ratio of styrene to maleic acid, and altSMA. The altSMA has an overall 2:1 ratio of styrene to maleic acid, but comprises a block of alternating S−MA with the excess styrene forming a polystyrene tail which is terminated by the DDMAT RAFT agent. (b) Model phase diagram schematic for a generic surfactant solubilizing a lipid, which we have applied to SMA solubilizing lipids into nanodiscs. At low surfactant concentrations, all the lipid exists in the bilayer phase as vesicles (V). At surfactant concentrations above the saturation boundary (SAT, blue dashed line), lipid is present as a combination of vesicles and micelles in the coexistence region (C). At surfactant concentrations above the solubilization boundary (SOL, red line), all lipid has been solubilized into surfactant−lipid micelles (M).

Recent work investigating the thermodynamic properties of the statistical SMA(3:1) polymer (with a styrene:maleic acid ratio of 3:1) and its assembly into nanodiscs has shown that the phase behavior of the solubilization can be approximated by a pseudophase model[36] (Figure 1b). Traditionally, the pseudophase model has been used to characterize the solubilization of phospholipids by surfactants.[36,37] When applied to SMA, the pseudophase model shows that upon increasing the concentration of SMA at a fixed concentration of lipid vesicles, three ranges can be identified: the bilayer range, the coexistence range and the micellar range (in the case of solubilization by SMA, the nanodisc range). The boundaries between these ranges are termed the saturation (SAT) and solubilization (SOL) boundaries. To allow comparison between SMA and classical surfactants, SAT and SOL boundaries can be expressed in terms of the molar ratio of surfactant to lipid at the phase boundary: $R_S^{b,SAT}$ and $R_S^{m,SOL}$, respectively (representing the gradient of the phase boundary line).[38] From these values, the Gibbs free energy change for the vesicle to nanodisc transition for lipids, $\Delta G_{lipid}^{b\rightarrow m,0}$, and for the solution to nanodisc transition for polymer, $\Delta G_{polymer}^{b\rightarrow m,0}$ can be calculated.

Since the first use of an SMA polymer (SMA2000, with a 2:1 ratio of S:MA) in membrane protein isolation,[39] a number of other SMA polymers have been shown to be effective in membrane solubilization.[40,36,41−43] These polymers have utilized different S:MA ratios and chain lengths. A recent side-by-side comparison of membrane protein solubilization by a number of these polymers has shown that their effectiveness varies significantly with the most effective remaining the original SMA2000 2:1 ratio polymer.[43]

In addition to effectiveness in membrane protein solubilization, thermodynamic studies of the solubilization of DMPC and POPC large unilamellar vesicles (LUVs) by an SMA(2:1) polymer have been reported.[44] These results demonstrated that this SMA(2:1) (Trade name Xiran SZ30010) is more efficient in membrane solubilization than the SMA(3:1) and this efficiency increases with increasing pH. These data, in combination with other studies,[45,46] have led to the emergence of SMA(2:1) polymers as the most effective solubilizer of membranes and membrane proteins.

In this work, we have therefore determined phase diagrams for the solubilization of DMPC vesicles using the acid forms of two SMA(2:1) polymers of differing chain length and chain topology, to investigate the effect of polymer structural properties on phospholipid solubilization. We compare the acid form of the commercially available and frequently utilized SMA2000 and a 2:1 SMA polymer synthesized using reversible addition−fragmentation chain transfer (RAFT) polymerization. RAFT-synthesized SMA has recently been shown to form nanodiscs with tunable properties based on the high degree of control over the polymerization that RAFT offers.[41] While SMA2000 is a statistical copolymer, RAFT-SMA has an alternating styrene-maleic acid block with the styrene excess forming a polystyrene tail terminating in the RAFT agent. This diblock approximation has however been shown to be an oversimplification of the RAFT-polymer structure. In reality, RAFT-synthesized SMA will display a gradient from alternating styrene-maleic acid toward polystyrene along the length of the polymer chain.[47] The polymers herein will be referred to as

DOI: 10.1021/acs.biomac.7b01539
Biomacromolecules 2018, 19, 761−772

Table 1. Thermodynamic Values Obtained for coSMA and altSMA Compared to SMA(3:1) and SMA(2:1) (Xiran SZ30010) Mediated Phospholipid Nanodisc Self-Assembly

	coSMA (SMA2000)	altSMA	SMA(2:1) (Xiran SZ30010)[44]	SMA(3:1) (Xiran SL25010 S25)[50]
M_w (kg·mol^{-1})	7.50	6.85	6.50	10.00
M_n (kg·mol^{-1})	3.00	6.00	2.70	4.00
$R_S^{b,\,SAT}$	0.050 ± 0.003	0.024 ± 0.002	0.087 ± 0.006	0.078 ± 0.002
$R_S^{m,\,SOL}$	0.133 ± 0.004	0.137 ± 0.007	0.130 ± 0.004	0.144 ± 0.001
$\Delta G_{lipid}^{b\rightarrow m,0}$ (kJ·mol^{-1})	+0.19 ± 0.06	+0.26 ± 0.08	+0.10 ± 0.02	+0.15 ± 0.05
$\Delta G_{polymer}^{b\rightarrow m,0}$(kJ·mol^{-1})	−2.23 ± 0.08	−4.11 ± 0.11	−0.91 ± 0.23	−1.36 ± 0.45

coSMA (SMA2000, acid form) and altSMA (RAFT-SMA, acid form). In addition to topological differences, these polymers also exhibit differences in chain length distribution to each other and to the Xiran SZ30010 SMA(2:1) studied by others. Here we have characterized the self-assembly and properties of SMALPs formed by coSMA and altSMA and compared to those formed by Xiran SZ30010 (as studied by others) in order to understand the factors that define the function of these materials.

Finally, we have confirmed that both polymers effectively solubilize membrane proteins directly from the *E. coli* cell membrane and assessed their performance in this regard relative to each other and to commonly used detergent alternatives.

EXPERIMENTAL SECTION

Materials. Figure 1a shows the structure of SMA2000 at pH 8.0 (poly(styrene-*co*-maleic acid)), purchased from Cray Valley (UK) as poly(styrene-*co*-maleic anhydride) (coSMAnh). All buffer components, chloroform, and 1,2-dimyristoyl-*sn*-glycero-3-phosphocholine (DMPC) were purchased from Sigma-Aldrich (UK) at >98% purity and used without further purification.

Methods. *Synthesis of altSMAnh.* altSMAnh with a styrene/maleic anhydride ratio of 2:1 and a molar mass of 6 kDa was synthesized using RAFT polymerization as described by Harrisson and Wooley.[48] altSMA was synthesized in one step by mixing initial reagents of styrene and maleic anhydride in a 2.34:1 ratio. Specifically, 1.0 g (9.6 mmol) of styrene and 0.404 g of maleic anhydride (4.1 mmol) were added in a molar ratio of 2.34:1 with 4.8 mg (0.03 mmol) of azobis(isobutyronitrile) (AIBN), and 72.2 mg (0.20 mmol) of 2-(dodecylthiocarbonothioylthio)-2-methylpropionic acid (DDMAT) was mixed in 4.4 mL of 1,4-dioxane and degassed by three freeze−pump−thaw cycles. The flask was slightly over pressured with nitrogen and maintained at 60 °C for 20 h. The viscous solution obtained was diluted in a minimal volume of THF and precipitated in diethyl ether before recovery by filtration. The redissolution and precipitation procedure was repeated three times and the resulting copolymer dried at 70 °C for 16 h. The molecular weight distribution was measured by size exclusion chromatography (Figure S1) and styrene:maleic anhydride ratio determined by NMR spectroscopy (Figure S2).

Nanodisc Preparation. coSMAnh and altSMAnh copolymers were hydrolyzed from the anhydride to the acid forms using a previously published procedure.[24] For a complete description, refer to the Supporting Information. Nanodiscs were prepared essentially as previously described.[35] In brief, DMPC was dissolved in chloroform and dried under nitrogen to create a multilamellar lipid film on the surface of the glass vial. Trace solvent was removed by placing overnight in a desiccator attached to a vacuum pump. DMPC was resuspended in 50 mM sodium phosphate pH 8 containing 200 mM NaCl to the required concentration for titration and concentration dependent experiments. Suspensions were sonicated for 30 min in a water bath at 35 °C to form small unilamellar vesicles (SUVs, presence confirmed by DLS). DMPC SUV suspensions were kept at room temperature and used within 3 days.

The molecular weight-averaged molar mass (M_w) and number-average molar mass (M_n) of the copolymers used in this study are shown in Table 1. We assume no changes of molecular weight on hydrolysis. Copolymer stock solutions were made in 50 mM sodium phosphate, 200 mM NaCl pH 8 to the required molar concentration required for titration experiments (calculated using the M_n value) or to 3% (w/v) if being used to make nanodiscs at excess copolymer concentration.

Nanodiscs were made by mixing 10 mg/mL DMPC suspension and 3% (w/v) copolymer solutions (or as required for titration and concentration dependent experiments) in a 1:1 ratio at room temperature. Nanodiscs were left at 25 °C for at least 24 h to equilibrate before use. For temperature stability experiments and freeze−thaw stability experiments, the resultant nanodiscs were purified using a Superdex S200 16/600 size exclusion chromatography column to remove large aggregates and excess polymer. Purified nanodiscs were concentrated using a 10 kDa MWCO spin concentrator to a copolymer concentration of 1.5% (w/v) determined by constructing a calibration curve of UV-absorbance at 254 nm for polymer solutions of known concentration.

^{31}P NMR. Lipid−polymer mixtures were prepared as described above with DMPC concentrations of 7.50, 5.00, 2.50, and 1.25 mM. For coSMA and altSMA experiments, instead of phosphate buffer (which would compromise the ^{31}P NMR signal from the lipids), 50 mM Tris pH 8.0, 200 mM NaCl was prepared in D_2O. All ^{31}P NMR experiments were performed using an Avance III 400 MHz NMR spectrometer (Bruker, Coventry, UK). Spectra were acquired at 298 K at 161.98 MHz using ^{1}H decoupling. Here, 256 scans were performed per measurement with an acquisition time of 1.022 s over a sweep width of 32 051 Hz. A prescan delay of 6.5 s, a relaxation delay of 5 s and a pulse width of 7.25 μs was required to observe sufficient signal on which to perform analysis. An external reference of 85% H_3PO_4 in 10% D_2O was measured and set to 0 ppm to correct for any drift of the magnetic field between experiments.

^{31}P NMR Data Analysis. TopSpin software (Bruker, Coventry, UK) was used to perform peak integration. Absolute integrals were then normalized to the largest and smallest value across all experiments. Peak area data were fitted using least-squares nonlinear regression.[49] In order to determine the saturating and solubilizing concentrations of copolymer for a given lipid concentration, fits to the experimental data were performed simultaneously to the following scenario:

$$A(c_S \le c_S^{SAT}) = 0 \tag{1}$$

$$A(c_S^{SAT} \le c_S \le c_S^{SOL}) = f c_L \frac{c_S - c_S^{SAT}}{c_S^{SOL} - c_S^{SAT}} \tag{2}$$

$$A(c_S^{SOL} \le c_S) = f c_L \tag{3}$$

where A represents peak area and c_S is the molar polymer concentration. c_S^{SAT} and c_S^{SOL} are the saturating and solubilizing concentrations of polymer for a given lipid concentration, c_L. f is a scaling factor dependent on data acquisition parameters.

Phase diagrams were constructed by plotting c_S^{SAT} and c_S^{SOL} as lipid concentration versus polymer concentration. Linear regression was performed to fit the following equations to the experimental data:

$$c_S^{SAT} = c_S + R_S^{b,SAT} c_L \tag{4}$$

$$c_S^{SOL} = c_S + R_S^{m,SOL} c_L \tag{5}$$

DOI: 10.1021/acs.biomac.7b01539
Biomacromolecules 2018, 19, 761−772

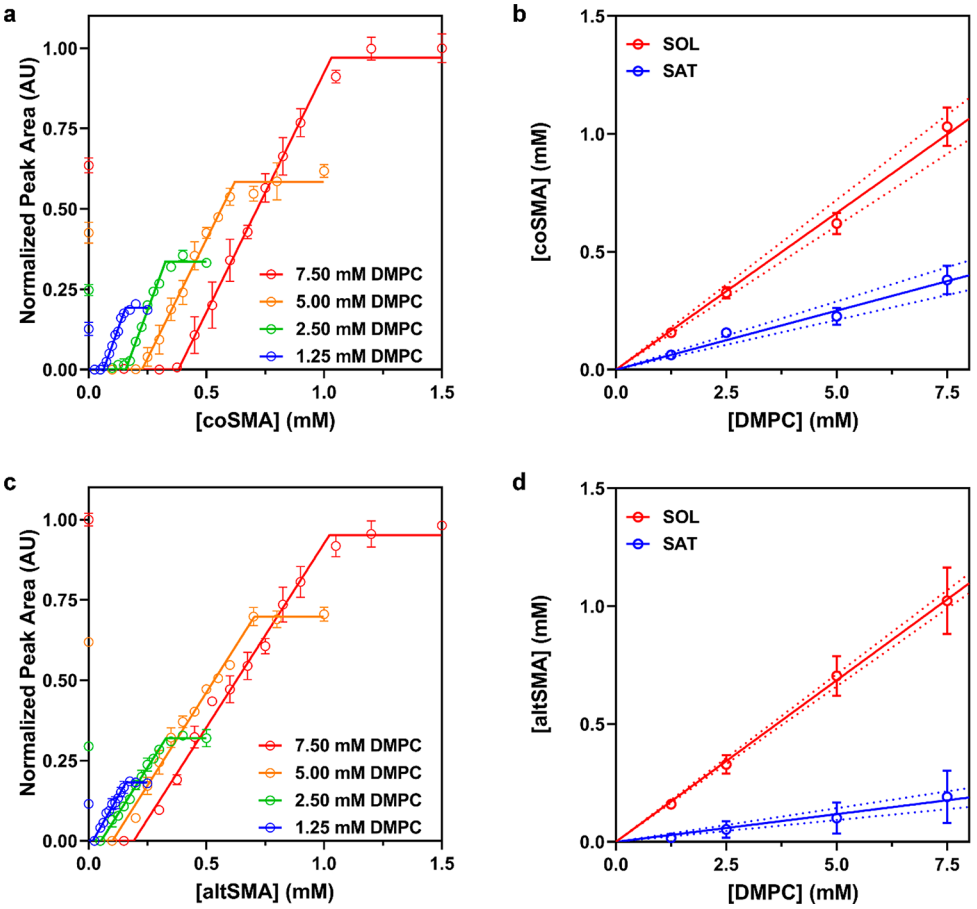

Figure 2. ^{31}P NMR Data for coSMA (a, b) and altSMA (c, d) solubilizing DMPC SUVs. (a, c) Normalized ^{31}P NMR peak area plotted as a function of polymer concentration with corresponding fits to the experimental data to obtain SAT and SOL break points. Each point is the mean of three separate measurements with error bars representing ±1 standard error. (b, d) Phase diagrams constructed using SAT and SOL breakpoints determined from (a) and (c). The SAT boundary is shown as a blue line and the SOL boundary is shown as a red line. Points represent c_S^{SAT} and c_S^{SOL} breakpoints with error bars representing the standard error determined from the fitting procedure in (a) and (c). Dashed lines represent the 95% confidence bands associated with linear regression.

where $R_S^{b,SAT}$ and $R_S^{m,SOL}$ represent the molar ratios of polymer to lipid at the SAT and SOL phase boundaries, respectively. This allows calculation of the partitioning coefficients:

$$K_{lipid}^{b\rightarrow m} = \frac{1 + R_S^{b,SAT}}{1 + R_S^{m,SOL}} \quad (6)$$

$$K_{polymer}^{b\rightarrow m} = K_{lipid}^{b\rightarrow m}\frac{R_S^{m,SOL}}{R_S^{b,SAT}} \quad (7)$$

for the lipid and polymer, respectively, between the vesicular bilayer phase (b) and the "micellar" (m) nanodisc phase. From this, the Gibbs free energy for the transfer from vesicular bilayer to nanodisc phase can be calculated for both the lipid:

$$\Delta G_{lipid}^{b\rightarrow m,0} = -RT\ \ln(K_{lipid}^{b\rightarrow m}) \quad (8)$$

And the polymer:

$$\Delta G_{polymer}^{b\rightarrow m,0} = -RT\ \ln(K_{polymer}^{b\rightarrow m}) \quad (9)$$

For a more complete theoretical description, see ref 36.

Dynamic Light Scattering. Dynamic light scattering experiments were performed with a Zetasizer Nano S (Malvern Instruments, Worcestershire, UK) using a He−Ne laser at 633 nm with a detector angle of 178° relative to the incident beam. Samples were loaded into 45 μL quartz cuvettes with a 3 × 3 mm light path (Hellma Analytics, Müllheim, Germany). All measurements were performed after equilibrating the sample at 25 °C for 60 s and each sample measured 3 times with the attenuator position automatically optimized for size determination. Each measurement consists of 11 scans of 10 s. Samples prepared for the concentration dependence of polymer were left to equilibrate for at least 3 h before the measurement. Freeze−thaw stability was performed by flash freezing the nanodisc solution in liquid N_2 for 5 min and then thawing at room temperature before being loaded into the cuvette. Temperature stability was performed by increasing the temperature from 4 to 80 °C in 1 °C increments. Again, each sample was measured three times at each temperature after equilibrating at that temperature for 2 min.

Size Exclusion Chromatography with Multiangled Light Scattering. SEC-MALS experiments were performed using a Superdex 200 increase 10/300 GL size exclusion column attached to an Äkta purification system (GE Healthcare Life Sciences, Buckinghamshire, UK). In line absorbance measurements at 280 and 254 nm were used to calibrate the delay volume between the column and the MALS detector. MALS measurements were performed using a Dawn Helios II (Wyatt Technologies, Suffolk, UK) equipped with a 633 nm He−Ne laser with static light scattering detectors positioned at 18 angles radially about the flow cell. The MALS detector at 110° has been replaced with a DLS detector in order to obtain information on the hydrodynamic radius of particles more accurately than using MALS alone. Samples were prepared as described above and centrifuged at 10,000*g* for 10 min to remove any contaminant particulate matter. A volume of 70 μL of each sample was loaded onto the column which was run with a flow rate of 0.7 mL/min.

DOI: 10.1021/acs.biomac.7b01539
Biomacromolecules 2018, 19, 761−772

Solubilization of Membrane Proteins from E. coli BL21 (DE3) Membranes. Membranes were resuspended to 60 mg/mL in 50 mM Na_2HPO_4, 0.2 M NaCl, 10% v/v glycerol pH 8 and homogenized. Stocks of 4% (w/v) Triton X-100, 2% (w/v) DDM, 2% (w/v) β-OG, 16 mM coSMA and 16 mM altSMA were prepared in 50 mM Na_2HPO_4, 0.2 M NaCl, 10% v/v glycerol pH 8. Membrane suspensions were mixed 1:1 with detergent or polymer samples and a control was performed where membranes were diluted to 30 mg/mL with in the same buffer but no detergent or polymer was added. All samples were incubated for 2 h (4 °C for control and detergent samples, 20 °C for polymer samples as per published protocols[24]). Samples were centrifuged at 100,000*g* for 45 min at 4 °C. The supernatant was removed containing the soluble fraction and the insoluble pellet resuspended in an equal volume of the same buffer. Soluble and insoluble fractions were then precipitated by the addition of 25% (w/v) trichloroacetic acid (TCA). After 10 min incubation at 4 °C, samples were centrifuged at 14,000*g* for 5 min to pellet precipitated protein. The protein pellet was washed three times by vortexing in 200 μL of ice cold acetone and repeating the centrifugation step. The protein pellet was dried under vacuum for 10 min before resuspension in the starting volume of buffer. The samples were analyzed by SDS polyacrylamide gel electrophoresis (PAGE) using precast Criterion XT graduated 4−12% acrylamide bis-tris gels (Bio-Rad Laboratorie Ltd., Hertfordshire, UK) using standard procedures and stained overnight using InstantBlue protein stain (Expedeon Ltd., Cambridgeshire, UK).

RESULTS AND DISCUSSION

Thermodynamics of Nanodisc Self-Assembly. In order to consistently compare measurements of nanodiscs formed from different polymers and lipids using different techniques, a thorough initial characterization of the nanodiscs is required. Vargas et al.[36] showed that ^{31}P NMR experiments could be used to determine the phase diagram of SMA(3:1) solubilizing vesicles of 1-palmitoyl-2-oleoyl-*sn*-glycero-3-phosphocholine (POPC). Similar experiments have also been performed by measuring the solubilization of DMPC vesicles by SMA(3:1)[50] and SMA(2:1) (Xiran SZ30010).[44]

We performed ^{31}P NMR experiments at 298 K to examine the phase diagram of coSMA and altSMA mediated solubilization of fluid phase DMPC small unilamellar vesicles (SUVs). The ^{31}P NMR peak from the phosphate group in DMPC did not broaden beyond detection as it does in the data published in ref 36 (Figure S4). This is due to the use of SUVs rather than large unilamellar vesicles (LUVs) as in the previous stud y.

Our data suggest the scenario proposed for the solubilization of POPC or DMPC LUVs by SMA(3:1)[36,50] and SMA(2:1) (Xiran SZ30010)[44] can also explain the solubilization of DMPC SUVs by coSMA and altSMA. At polymer concentrations below c_S^{SAT}, the ^{31}P peak broadens beyond detection as the polymers embed in the vesicular bilayer. The initial decrease in peak area suggests that the rearrangement of SUVs into larger, slower tumbling structures, occurs through individual polymer chains cross-linking vesicles, or polymer chains adsorbing into the vesicular bilayer leading to a swelling of the vesicle. As c_S^{SAT} is surpassed, the polymer molecules are able to initiate the bilayer to nanodisc phase transition. This leads to a sharp, linear increase in ^{31}P NMR peak area as lipids become solubilized into small, fast tumbling nanodiscs. Above c_S^{SOL}, there is sufficient polymer present to solubilize all lipids into nanodiscs, so further increases in peak areas are not observed.

In all experiments, fitting of the ^{31}P peak area yields c_S^{SAT} and c_S^{SOL} values, which are proportional to the DMPC concentration. Therefore, plotting these breakpoints as polymer concentration vs DMPC concentration allows us to obtain phase diagrams (Figure 2b, d). From these, we calculated the molar ratios of polymer to lipid at each of the phase boundaries (Table 1). coSMA has a noticeably larger $R_S^{b,\,SAT}$ value (steeper gradient of blue lines in Figure 2b) compared to altSMA (Figure 2d), indicating that over twice the molar concentration is required to saturate a given quantity of DMPC. In contrast, coSMA and altSMA have almost identical $R_S^{m,\,SOL}$ values (the gradients of the red lines in Figures 2b and d). This means that, although altSMA is more effective at starting the solubilization of DMPC, both polymers ultimately require similar concentrations to achieve complete solubilization. It is worth noting that all of the values derived for these polymers, including $R_S^{m,\,SOL}$, are lower than previously determined for SMA(3:1). This means that the statistical SMA(3:1) is less effective in nanodisc self-assembly than both SMA(2:1) polymers investigated. SMA(2:1) Xiran SZ30010 shows very similar molar ratios of polymer to lipid at the solubilization boundary to both coSMA and altSMA. This points at an overriding influence of chemical composition of the SMA copolymers compared to chain topology.

Table 1 also shows the Gibbs free energy change for the vesicle to nanodisc transition. In all cases, the relatively large negative free energy change associated with this transition for each polymer indicates that the polymer−lipid complex is significantly thermodynamically favored. It also shows that altSMA exhibits a more negative free-energy change associated with the vesicle to nanodisc transition than coSMA. This is probably due to the topological differences between the polymers. We expect that the hydrophobic polystyrene tail present on altSMA experiences a larger driving force to bury itself in a hydrophobic environment than the statistical ordering of styrene and maleic acid moieties on coSMA. The RAFT agent used to make this polymer may also have an effect here, although we do not have any data to quantify such an effect. Further, altSMA has a much narrower mass distribution than the commercial copolymers. Therefore, there are far fewer less thermodynamically favorable small chains present which could account for the larger thermodynamic driving force compared to the commercial copolymers.

The relatively small positive Gibbs energy change for DMPC undergoing the vesicle to nanodisc transition in all cases shows that from the lipids' perspective there is little energetic cost in going from a vesicle into a SMALP and the major driving force for this process is the large gain from the polymer. Comparing this with SMA(3:1) (where DMPC LUVs were solubilized at 30 °C) suggests that while DMPC molecules are in a more favorable free-energy environment within SMA(3:1)-SMALPs, the SMA(3:1) polymer has a much smaller thermodynamic driving force for self-assembly into SMALPs.

It is particularly notable that the magnitude of the free energy change for the two polymers studied here is significantly larger than that seen in previous studies, and particularly in comparison with Xiran SZ30010 (where again, DMPC LUVs were solubilized at 30 °C) which has the same ratio of styrene to malic acid. When taking into account the molar mass distributions of the copolymers, Xiran SZ30010 has the smallest M_n and M_w compared to coSMA, altSMA and SMA(3:1), and it is the least thermodynamically efficient polymer of those tested. This points to an interplay between the more efficient 2:1 styrene to maleic acid ratio, and the more thermodynamically effective longer copolymer chains and topologies for optimum phospholipid solubilization. This may explain why in

DOI: 10.1021/acs.biomac.7b01539
Biomacromolecules 2018, 19, 761−772

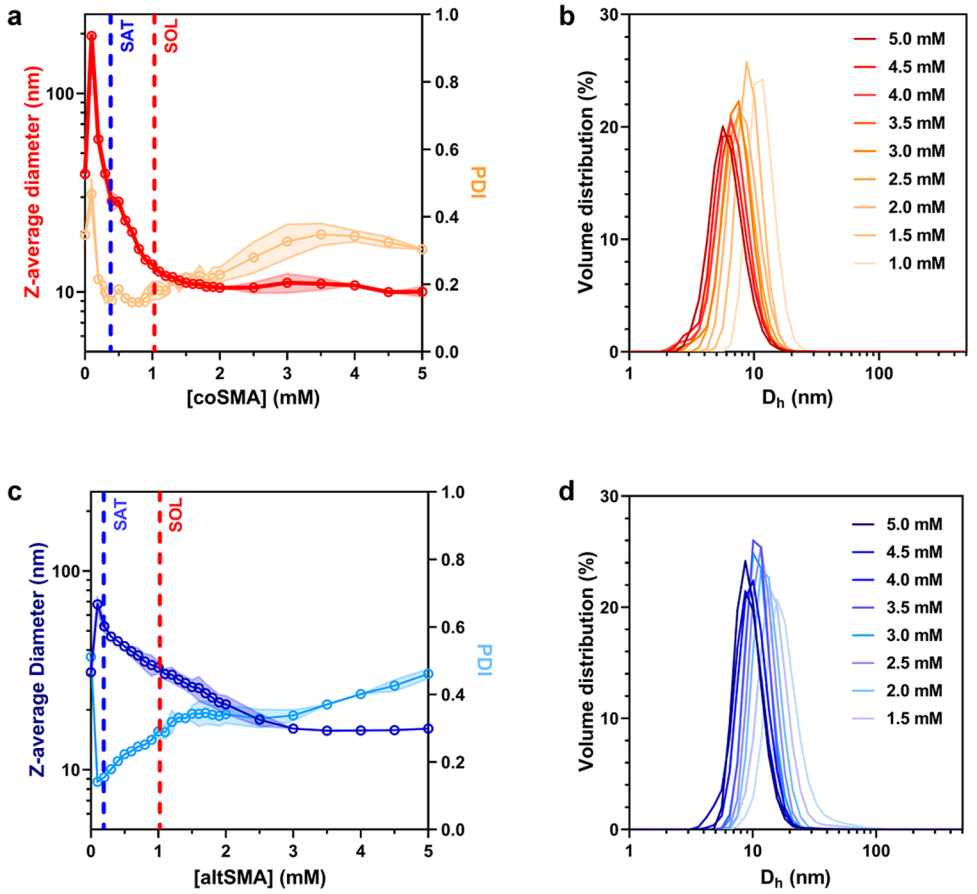

Figure 3. (a, c) DLS data showing the effect of coSMA (a), altSMA (c) concentration on *Z*-average diameter (dark line) and polydispersity index (PDI, light line). SAT and SOL boundaries obtained from ^{31}P NMR are shown as dashed blue and red lines respectively. Points represent the mean and shaded regions indicate the standard error obtained from three separate experiments. (b, d) Volume weighted particle size distribution (PSD) data showing the hydrodynamic diameter (D_h) for SMALPs formed at coSMA (b) and altSMA (d) concentrations above c_S^{SOL}. Lines represent the mean PSD of three separate experiments. Error bars are not shown for clarity.

comparisons of SMALP solubilization effectiveness and downstream stability, coSMA is more effective than other related polymers.[43]

Controlling the Size of Nanodiscs Formed by coSMA and altSMA. Next, we undertook structural characterization of nanodiscs by dynamic light scattering (Figure 3) to monitor *Z*-average diameters, associated polydispersity indices and volume weighted particle size distributions as a function of polymer concentration. Both coSMALP and altSMALP self-assembly show very similar trends across the measured polymer concentration range. Initially, where $c_S \leq c_S^{SAT}$, both coSMA and altSMA show an increase in *Z*-average diameter and corresponding drop in polydispersity. This is in agreement with volume weighted particle size distribution (PSD) data (Figure S5) which show a shift toward larger diameters upon the addition of 0.1 mM of polymer to a 7.5 mM DMPC SUV suspension. This occurs below c_S^{SAT}, correlating to the previously discussed broadening of ^{31}P NMR peak, so a possible explanation is incomplete polymer insertion leading to polymer chain cross-linking between vesicles and thereby forming an effectively larger species. Interestingly, coSMA induces aggregation of vesicles leading to a *Z*-average diameter >100 nm, whereas altSMA induces aggregation <80 nm. In both cases, as c_S^{SOL} is approached the *Z*-average diameter shrinks as the vesicles become solubilized. AltSMA induces a much more gradual decrease in *Z*-average diameter compared to coSMA. However, both polymers lead to a gradual increase in polydispersity beyond c_S^{SAT}. These data show that there are no well-defined structural changes occurring at each of the previously determined thermodynamic breakpoints. A similar phenomenon was observed with SMA(3:1) solubilizing POPC vesicles.[36] Under the conditions used, ^{31}P NMR is sensitive only to small, fast-tumbling particles so exclusively monitors the formation of SMALPs, while DLS is able to track the net changes in particle diameter and is most sensitive to larger particles, which can mask the onset of SMALP formation where the majority of lipid is not present within a smaller nanodisc structure.

Increasing c_S beyond c_S^{SOL} leads to a steady decrease in *Z*-average diameter (Figure 3a, c) and shifting of the PSD toward smaller diameters (Figure 3b, d) over the concentration range measured. From c_S^{SOL} to 5 mM polymer concentration, coSMALPs decreased in diameter from 14.6 ± 0.3 to 10.0 ± 0.8 nm, a 31% decrease in size, while altSMALPs decreased in diameter from 30.3 ± 1.9 to 16.1 ± 0.3 nm, decreasing in diameter by 53%. This trend has been observed with other SMA polymers,[36,44] although occurs to a greater extent with altSMA to previously studied polymers.

The increasing PDI above c_S^{SOL} is related to the addition of excess polymer. Polymer can either remain free in solution or interact with existing nanodiscs, both of which would modify the PDI. altSMA should also be able to self-assemble into

DOI: 10.1021/acs.biomac.7b01539
Biomacromolecules 2018, 19, 761−772

micelles in the absence of lipid due to the presence of the hydrophobic polystyrene tail which could again influence the PDI. We believe that the dominant factor in decreasing the *Z*-average diameter upon increasing polymer concentration is not the presence of particulate free polymer in solution, but the formation of an increased number of nanodiscs. This is because, for both polymers, as the polymer concentration is increased, we see a clear shift in the peak position without an associated broadening. This indicates a decrease in the disc diameter but only a small change in polydispersity. Furthermore, the negative Gibbs free energy change associated with the polymers during nanodisc self-assembly indicates that the polymers will preferentially interact with lipids over self-interaction.

If this interpretation is correct, it means that we see the formation of a greater number of nanodiscs at polymer concentrations above c_S^{SOL}. We believe lipid reorganization between nanodiscs is a dynamic process because lipid exchange has been observed elsewhere[51,52] and we have no reason to believe that is not the case here. Therefore, for higher polymer concentrations, we would expect the available lipids to be distributed among the polymer in such a way as to minimize the Gibbs free energy, and this would result in fewer lipids being present per nanodisc, explaining the observed decrease in size. This interpretation would also explain our assertion (mentioned earlier) that the chemical shift seen with ^{31}P NMR data is partly due to interaction of a greater number of DMPC head-groups with the polymer belt beyond c_S^{SOL}.

Previous experiments have shown that one can vary the size of nanodiscs by changing the styrene:maleic acid ratio of the SMA polymer.[41] The data presented here indicate polymers with the same styrene:maleic acid ratio are able to form nanodiscs with different size ranges; altSMALPs appear larger than coSMALPs at equivalent molar polymer concentrations beyond c_S^{SOL}. However, these data do not confirm whether it is the chain topology which leads to the observed differences in diameter because changes in polymer chain length may also lead to this effect. coSMA has a broader chain length distribution and a far greater proportion of small chains compared to altSMA (Table 1). The larger proportion of shorter chains in coSMA could also lead to the observed difference in size distributions. However, a recent investigation of RAFT-synthesized SMA polymers found no significant change in SMALP diameter formed using polymers of the same monomer ratio but different chain lengths.[41] This indicates that the observed size difference between coSMALPs and altSMALPs is due to differences in polymer topology rather than size distribution. When comparing SMALPs assembled using statistical 2:1 and 3:1 SMA polymers, the nanodiscs are of a similar size. This is a different trend to that seen with RAFT-synthesized polymers where 3:1 polymers have been shown to have a decreased diameter when compared to 2:1 polymers.[41] SMALP size is therefore likely driven by the relative proportion of poly(styrene) and poly(styrene-*alt*-maleic acid) blocks of the polymer chain. Nonetheless, these data provide evidence that the nanodisc size can be tuned by simply changing the polymer concentration above c_S^{SOL}.

Molecular Weight Determination of Nanodiscs. DLS data suggest that at polymer concentrations beyond c_S^{SOL}, excess polymer may exist as free polymer in solution or may associate with existing SMALPs. We therefore performed SEC-MALS measurements to assess what populations of species are present in solution at polymer concentrations in excess of c_S^{SOL} with the same number of monomer units (5 mg·mL^{-1} DMPC, 1.5% (w/v) polymer), and to determine molecular weights of coSMALP and altSMALP nanodiscs (Figure 4).

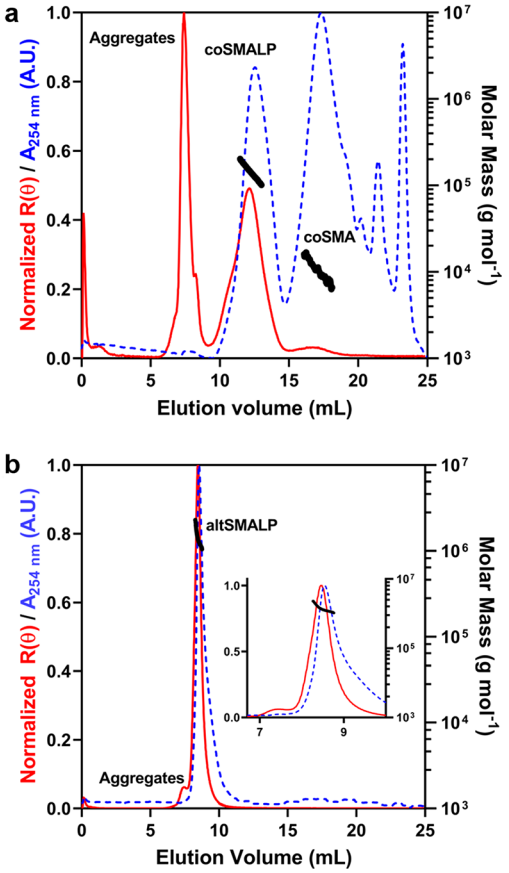

Figure 4. SEC-MALS chromatograms corresponding to (a) coSMALP and (b) altSMALP nanodiscs containing DMPC. Traces show the normalized Rayleigh ratio (red) and UV absorbance at 254 nm (blue, dashed) with overlaid mass calculations (black points). (b) Inset displays an expanded *X*-axis to allow for clearer distinction between the aggregate and altSMALP peak.

SEC-MALS analysis of coSMALPs (Figure 4a) show three principal features that appear with increasing elution volume. The first large aggregate peak (at 8 mL elution volume just after the void volume) detected by light scattering has no UV absorbance at 254 nm. The lack of UV absorbance suggests that this peak is due only to aggregated DMPC in a state which does not interact with the polymer. The second feature (which we have designated as "coSMALP" in Figure 4a) is detected by both light scattering and UV absorbance, showing a symmetric Gaussian-like shape. Analysis of in-line DLS data (Table 2) indicates a hydrodynamic diameter of ∼10 nm, similar to that determined by DLS independently. Analysis of MALS data (Table 2) shows a large mass and low polydispersity. Furthermore, ratio of the radius of gyration (R_g) from MALS and the hydrodynamic radius (R_h) from in-line DLS gives information on particle shape.[53] For this peak the ratio is in the range of oblate spheroids, consistent with a disc structure proposed. However, this conclusion should be treated with some caution because the small size of the particles means that the R_g determined by MALS is not wholly reliable as an absolute value and should only be considered indicative of the particle shape. We therefore assign this peak to DMPC/coSMALP nanodiscs. The final feature in the SEC-MALS

DOI: 10.1021/acs.biomac.7b01539
Biomacromolecules 2018, 19, 761−772

Table 2. Parameters Determined by Analysis of SEC-MALS Data Collected from DMPC coSMALPs and altSMALPs

	coSMALPs		altSMALPs
	coSMALP peak	coSMA peak	altSMALP peak
hydrodynamic diameter (nm)	9.45 ± 0.13	3.67 ± 0.23	25.00 ± 0.36
R_g (nm)	5.50 ± 0.64	8.17 ± 0.92	13.93 ± 0.49
R_g/R_h	1.16 ± 0.12	4.45 ± 0.39	1.11 ± 0.03
M_w (kDa)	146.13 ± 2.93	11.29 ± 0.51	1512 ± 84
M_n (kDa)	142.70 ± 2.93	10.89 ± 0.63	1488 ± 88
$Đ$	1.02 ± 0.01	1.04 ± 0.01	1.02 ± 0.01

chromatogram (designated as "coSMA" in Figure 4a) shows a large UV absorbance but only a small scattering intensity. The hydrodynamic diameter is smaller and has a significantly lower mass than the coSMALP peak, with an R_g/R_h ratio in the range of a prolate spheroid or rod, which is consistent with bundled, extended polymer chains. This is supported by SEC-MALS analysis of coSMA in the absence of lipids (Figure S6a, Table S1) which gives similar results. Here, a larger polymer aggregate is present in addition to the peak we have assigned as rod-like polymer bundles. Further downstream peaks show no scattering intensity with only UV absorbance and are highly convoluted. These peaks are also present for coSMA in the absence of lipids. We propose that these peaks are due to excess polymer that has not formed higher order structures in solution.

In contrast, altSMALPs show much cleaner SEC-MALS chromatogram (Figure 4b). There is only a small peak at the void volume (inset to Figure 4b) detected by light scattering (assigned to lipid aggregates) followed by a single sharp peak detected by UV-absorbance and light scattering, which we assign to nanodiscs. Again, this assignment is supported by an R_g/R_h ratio, very similar to that of coSMALPs, in the range of oblate spheroids. At higher elution volumes, there are only very minor UV peaks corresponding to excess free polymer in solution. As altSMA was added in excess of c_S^{SOL}, one would expect to see a large UV signal arising from free polymer in solution. The absence of this signal suggests that either all altSMA is associating with nanodiscs, or excess altSMA is forming lipid-free structures of a similar size to DMPC/altSMALPs that cannot be resolved. SEC-MALS analysis of altSMA in the absence of lipids shows a peak detected by light scattering and UV-absorbance that does indeed elute at the same elution volume as altSMALPs. The R_g/R_h ratio across this peak is consistent with a spherical particle (Figure S6b). The peak corresponding to altSMALP nanodiscs shows a hydrodynamic radius of 25 nm which is in the range measured using stand-alone DLS discussed above. The measured molecular weight is on the order of 10-fold higher than calculated for coSMALPs. Assuming a cylindrical structure, the mass of altSMALPs would be expected to be 7-fold higher than coSMALPs given the measured hydrodynamic radii of the two particles. This suggests that in the case of altSMALPs, altSMA in solution will associate with the available DMPC to form nanodiscs and thereby minimize the Gibbs free energy, rather than remain as spherical micelle-like particles. Such a conclusion is supported by the R_g/R_h values. The polydispersity for the altSMALP peak gives the same value as measured for coSMALPs.

Stability of Nanodiscs. A lot of recent interest in SMALPs from the membrane protein community is due to the increased stability of the solubilized target protein over classical "head and tail" detergents.[26,43] It is therefore of interest to understand how robust these nanodiscs are to temperature and particularly to the freezing process. We used DLS to measure changes in Z-average diameter as a function of temperature between 4 to 80 °C (Figures 5a and S7).

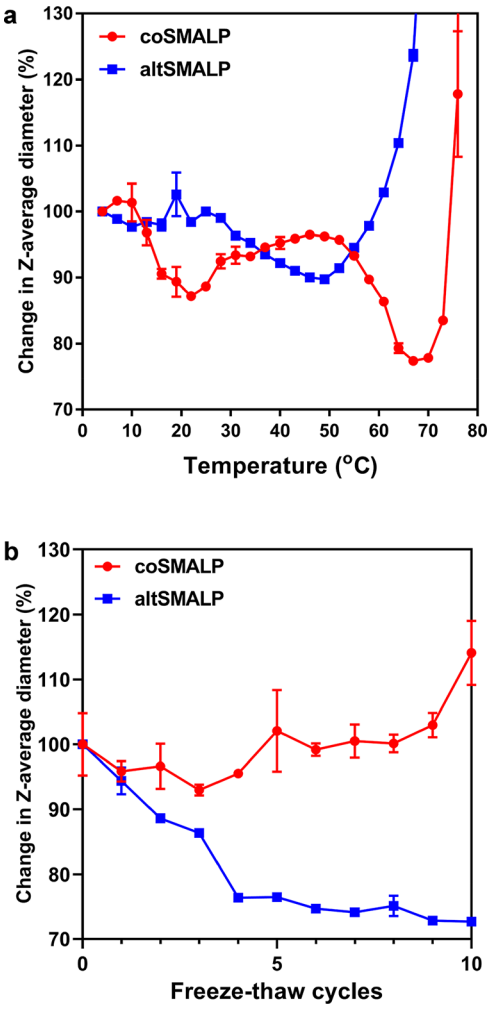

Figure 5. DLS data showing the effect of temperature (a, for clarity every third data point is plotted) and freeze−thaw cycles (b) on Z-average diameter of SEC purified coSMALP (red circles) and altSMALP (blue squares) nanodiscs containing DMPC. Points represent the mean value taken from three separate experiments with error bars displaying ±1 standard error. In order to highlight changes, the data plotted in (b) are shown as a percentage, rather than the absolute diameter (which are plotted in Figure S7 in the Supporting Information).

At low temperatures (from 4 to 12 °C), DMPC coSMALPs appear at a Z-average diameter of 10.6 ± 0.5 nm. Between 13 and 20 °C they then show a gradual decrease in diameter to 9.3 ± 0.2 nm. The onset of this decrease in size is of interest as 13 °C is known to be the pretransition temperature for pure DMPC (gel to ripple phase).[54,55] From 20 to 50 °C, the nanodiscs slowly increase in diameter to 10.1 ± 0.1 nm. It is again worth noting that this increase begins approximately after the melting phase transition for pure DMPC at 24 °C. From 50

DOI: 10.1021/acs.biomac.7b01539
Biomacromolecules 2018, 19, 761−772

to 68 °C, coSMALPs significantly shrink in size by about 20% (to 8.0 ± 0.03 nm) and then above 68 °C, we observe a rapid increase in *Z*-average diameter.

It is difficult to fully explain these observations on a microscopic level, though we can speculate. The initial decrease in diameter may be related to small losses of lipids from the nanodiscs that result from increased thermal motion of the DMPC tails. Above 24 °C, DMPC is in the liquid phase, so increased mobility of DMPC molecules may exert outward pressure on the polymer belt that more than compensates for any losses of lipids from the discs and so lead to an increase in size. At higher temperatures still, this can no longer compensate for lipid loss and so the discs shrink again until they start to aggregate above 68 °C.

At low temperature, the altSMALPs are observed to be 21.0 ± 0.03 nm and, in contrast to coSMALPs, do not show any significant change in diameter until 24 °C. Above this temperature a gradual decrease in size is observed to a minimum of 18.7 ± 0.1 nm at 47 °C. We have no reason to suspect the mechanism leading to this diameter change is different to coSMALPs. Above this temperature, the size of the altSMALPs increase significantly with increasing temperature. *Z*-Average diameter data could not be measured above 75 °C for coSMALPs or altSMALPs as a precipitated lipid film deposited on the inside of the cuvette. Lowering the temperature did not result in resolubilization of this precipitate. While high temperature destabilizes both coSMALPs and altSMALPs, both occur above usual working ranges, within which they are of comparable thermal stability.

We have also used DLS to characterize changes in coSMALPs and altSMALPs as a function of the number of freeze−thaw cycles (Figures 5b and S7). Volume PSD data for all nanodiscs clearly show that there are no aggregation effects or large changes in hydrodynamic diameter after 10 freeze−thaw cycles (Figure S8). Looking at *Z*-average diameter data (Figures 5b and S7) there is a broad trend of increasing diameter for coSMALPs through repeated freeze−thaw cycles. This trend is quite poorly defined; the diameter shows an initial small decrease but is approximately constant until 8−10 cycles where the increase becomes more obvious. The coSMALP diameter is 114% of the original size after 10 freeze−thaw cycles, increasing from 11.45 ± 0.95 to 13.06 ± 0.97 nm. In contrast, the altSMALPs show a much more pronounced decreasing diameter with increasing number of cycles, with an altSMALP diameter of 76% of their original size after 10 freeze−thaw cycles, decreasing from 17.93 ± 0.14 to 13.03 ± 0.16 nm. The majority of the size reduction appears over the first few cycles and the particle size appears to show relatively much smaller changes thereafter. To explain these observations, we speculate that multiple freeze−thaw cycles could lead to a minor lipid loss in altSMALPs as discussed above. coSMALPs seem to be much less affected by freeze−thaw cycles. This leads us to suspect that it is the poly(styrene) tail of altSMA which is expected to bury in the core of the nanodisc and could disrupt the lipids to a greater extent than coSMA, leading to the observed increased susceptibility to structural changes upon multiple freeze−thaw cycles.

It is worth nothing that analysis of DLS data assumes a spherical particle and since we believe that neither coSMALPs or altSMALPs are spherical structures, the validity of the assumptions used to draw conclusions on the size of the particles is somewhat limited. The apparent small changes in diameter from DLS could alternatively be due to more complicated changes in the overall particle dimensions, swelling of the bilayer region, for example.

Solubilization of Membrane Proteins. Thus far, we have only characterized the various nanodiscs using a model DMPC bilayer. As a primary use of these polymers will be to solubilize membrane proteins, we have also tested their ability to solubilize proteins from isolated *E. coli* BL21(DE3) membranes. As controls we have compared the polymers to some common traditional detergents: Triton X-100, *n*-dodecyl *β*-D-maltopyranoside (DDM) and octyl *β*-D-glucopyranoside (*β*-OG) as well as a sample where no detergent was added (Figure 6).

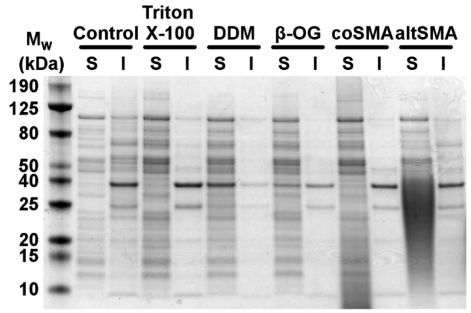

Figure 6. Coomassie stained SDS-PAGE showing the range of proteins that have been solubilized (S) and remained insoluble (I) after the incubation of *E. coli* membranes with coSMA and altSMA compared to three traditional detergents (Triton X-100, DDM and *β*-OG) and a control where no detergent was added to the membrane extract.

The experiment shows that coSMA is able to solubilize the membrane proteome with comparable efficiency to traditional detergents and significantly better than the control experiment without detergent. altSMA also shows a clear improvement over the detergent-free control though it is less effective than coSMA and traditional detergents. Interestingly, altSMA induces a loss of resolution on SDS-PAGE. We speculate that this is due to altSMA to forming larger polymer aggregates which migrate through the gel and thus leads to a loss of resolution.

Given the different sizes of nanodisc formed by each polymer, there does not appear to be any selectivity toward proteins of different masses, with each polymer effectively solubilizing proteins across the whole mass range. However, given that altSMA displays a decreased extraction efficiency, it appears that the alternating topology combined with the hydrophobic polystyrene tail is, in this case, less effective when extracting membrane proteins from native *E. coli* membranes. We speculate that the polystyrene tail present on altSMA may bury itself within the acyl region of the lipid bilayer and could therefore interact with hydrophobic membrane spanning regions of certain membrane proteins. This interaction could prevent a clean solubilization of membrane proteins. This hypothesis is supported by previous observations where RAFT-synthesized SMA copolymers with a long polystyrene tail have been ineffective in solubilizing membrane proteins.[47] Nonetheless, altSMA is able to form nanodiscs up to twice the diameter of coSMA (as shown above). Previous analysis of SMALP structure formed by coSMA has led to the estimate of a maximum of 40 *α*-helices being able to pack into the lipid core of a SMALP.[23] If one assumes that the lipid core of altSMALPs increases in diameter proportionately to the overall particle

DOI: 10.1021/acs.biomac.7b01539
Biomacromolecules 2018, 19, 761−772

diameter, then altSMA may have useful application in the extraction of larger membrane protein complexes which are too large to be encapsulated by coSMA.

CONCLUSIONS

It is becoming increasingly clear that the SMALP system offers significant advantages over detergent-based systems for membrane protein production. The retention of the membrane solvating the membrane protein assures near native structure, function and stability. In addition, unlike detergent systems there is no need to maintain a concentration of free SMA above a nominal CMC meaning less issues with interference with downstream applications. However, it is clear that the rapid adoption of the SMALP method has outreached our fundamental understanding of the process of SMALP formation. While pragmatically this is not an issue as a number of SMA 3:1 and 2:1 polymers function adequately as membrane protein solubilizers, it is likely that at some point improved polymers are going to be required. To generate these polymers in a targeted fashion, an understanding of the SMALP formation process and the influence of polymer structure is going to be required. In this study we have applied methods developed for the study of other SMA polymers to the original SMA polymer (SMA2000) used in the first demonstration of SMALPs in membrane protein isolation[39] that has remained the most effective membrane protein solubilization polymer.[43] With the addition of data from a related RAFT polymer and in combination with data from three other studies of related polymers[36,44,50] we can begin to correlate polymer structure with effectiveness in membrane protein solubilization.

Both coSMA and altSMA exhibit a stronger thermodynamic driving force for nanodisc self-assembly than the SMA(2:1) (Xiran SZ30010) and SMA(3:1). This has demonstrated that at least four parameters (polymer chain length, chain length distribution, topology and monomer ratio) have influence on the SMALP self-assembly process. This correlates well with published data which show that these parameters have influence on the capability of the SMA to extract membrane proteins.[43] We have identified SMA polymers with a 2:1 styrene/maleic acid ratio being the most efficient in membrane solubilization and polymers of larger length displaying the more favorable free energy change associated with SMALP formation among those tested. We have shown that changing the topological structure of polymers with the same 2:1 styrene/maleic acid ratio causes large differences in SMALP size and molecular weight. Furthermore, by simply increasing the polymer concentration beyond c_S^{SOL}, the final size of the nanodiscs can be further tuned. We have shown that coSMALPs and altSMALPs are of comparable stability, and able to effectively solubilize membrane proteins from the *E. coli* membrane, though with subtle differences. Previous studies have found that SMA polymers with a lower styrene content, similar to the poly(styrene-*alt*-maleic acid) block of altSMA, have been ineffective in forming SMALPs and extracting membrane proteins.[43,47] This leads us to believe that the presence of the polystyrene tail on altSMA is driving the differences observed in comparison to coSMA. The *S*-dodecyl trithiocarbonate end group is likely to hydrolyze under the conditions employed for ring-opening of the maleic anhydride (2 h, 100 °C, 1 M NaOH), and yield a thiol end group. It however cannot be ruled out that a certain fraction of the dodecyl end groups are retained at the chain end, and contribute to the hydrophobicity of the polystyrene tail of the copolymer. Lack of trithiocarbonate end group hydrolysis has previously been reported, albeit under milder conditions (16 h, room temperature, 0.1 M NaOH).[41] Other classes of RAFT agent could be used[56] which could potentially be exploited to modify the properties of resultant SMALPs. This work indicates that SMALPs can be formed with varying properties, which can be applied to membrane and membrane protein research. These, and further modifications to the SMA polymer will expand the capabilities of the SMA tool kit.

ASSOCIATED CONTENT

Supporting Information

The Supporting Information is available free of charge on the ACS Publications website at DOI: 10.1021/acs.biomac.7b01539.

Experimental details for polymer hydrolysis, DLS data analysis, SEC-MALS data analysis and isolation of *E. coli* (BL21)DE3 membranes; size exclusion chromatography (SEC) and NMR characterization of RAFT-synthesized altSMAnh; UV−vis spectra for both coSMA and altSMA; raw ^{31}P NMR spectra obtained for the titration of copolymers into DMPC SUV suspensions; DLS data showing PSDs of structures formed at copolymer concentrations below c_S^{SOL}; SEC-MALS analysis of coSMA and altSMA in the absence of phospholipids; DLS data showing the thermal stability of coSMALPs and altSMALPs; DLS data showing PSDs of SMALPs through sequential freeze−thaw cycles (PDF)

AUTHOR INFORMATION

Corresponding Author

*E-mail: tom.arnold@diamond.ac.uk.

ORCID

Bert Klumperman: 0000-0003-1561-274X

Karen J. Edler: 0000-0001-5822-0127

Thomas Arnold: 0000-0001-8295-3822

Present Address

#European Spallation Source ERIC, P.O Box 176, SE-221 00 Lund, Sweden.

Author Contributions

The manuscript was written through contributions of all authors. All authors have given approval to the final version of the manuscript.

Notes

The authors declare no competing financial interest.

ACKNOWLEDGMENTS

The authors wish to thank S. Keller and R. Cuevas for invaluable discussions on drafts of this manuscript and particularly advice regarding ^{31}P NMR experiments. SH wishes to thank G. Harris, I. Walmsby and T. J. Knowles for assistance with ^{31}P data collection. We also thank the ISIS spallation source, L. Clifton and A. Dopplapudi for access to DLS and D_2O required for NMR experiments, and the Research Complex at Harwell and David Scott for access to ^{31}P NMR spectroscopy and SEC-MALS. This work has been supported by an EPSRC and Diamond Light Source studentship for SH (EP/M506461/1; studentship agreement STU0130) and BBSRC funding (BB/M018261/1 & BB/J017310/1).). CT acknowledges STFC BioMemNet (studentship agreement #2990) and the University of Bath for PhD studentship

DOI: 10.1021/acs.biomac.7b01539
Biomacromolecules 2018, 19, 761−772

funding, and the University of Bath and Stellenbosch University for travel funding to Stellenbosch University. BK thanks support by the South African Research Chairs Initiative of the Department of Science and Technology (DST) and National Research Foundation (NRF) of South Africa (Grant No 46855).

■ ABBREVIATIONS

SMA, poly(styrene-*co*-maleic acid); SMAnh, poly(styrene-*co*-maleic anhydride); SMALP, SMA lipid particle; RAFT, reversible addition−fragmentation chain transfer; DMPC, 1,2-dimyristoyl-*sn*-glycero-3-phosphocholine; SUV, small unilamellar vesicle; LUV, large unilamellar vesicle; NMR, nuclear magnetic resonance; DLS, dynamic light scattering; PSD, particle size distribution; PDI, polydispersity index; SEC-MALS, size exclusion chromatography with multiangled light scattering; PAGE, poly(agarose) gel electrophoresis.

■ REFERENCES

(1) Almén, M. S.; Nordström, K. J. V.; Fredriksson, R.; Schiöth, H. B. Mapping the Human Membrane Proteome: A Majority of the Human Membrane Proteins Can Be Classified According to Function and Evolutionary Origin. *BMC Biol.* **2009**, *7*, 50.

(2) Tan, S.; Tan, H. T.; Chung, M. C. M. Membrane Proteins and Membrane Proteomics. *Proteomics* **2008**, *8* (19), 3924−3932.

(3) Fagerberg, L.; Jonasson, K.; von Heijne, G.; Uhlén, M.; Berglund, L. Prediction of the Human Membrane Proteome. *Proteomics* **2010**, *10* (6), 1141−1149.

(4) Overington, J. P.; Al-Lazikani, B.; Hopkins, A. L. How Many Drug Targets Are There? *Nat. Rev. Drug Discovery* **2006**, *5* (12), 993−996.

(5) Stansfeld, P. J.; Goose, J. E.; Caffrey, M.; Carpenter, E. P.; Parker, J. L.; Newstead, S.; Sansom, M. S. P. MemProtMD: Automated Insertion of Membrane Protein Structures into Explicit Lipid Membranes. *Structure* **2015**, *23* (7), 1350−1361.

(6) Carpenter, E. P.; Beis, K.; Cameron, A. D.; Iwata, S. Overcoming the Challenges of Membrane Protein Crystallography. *Curr. Opin. Struct. Biol.* **2008**, *18* (5), 581−586.

(7) Moraes, I.; Evans, G.; Sanchez-Weatherby, J.; Newstead, S.; Stewart, P. D. S. Membrane Protein Structure Determination — The next Generation. *Biochim. Biophys. Acta, Biomembr.* **2014**, *1838* (1), 78−87.

(8) Smith, S. M. Strategies for the Purification of Membrane Proteins. In *Protein Chromatography*; Walls, D., Loughran, S. T., Eds.; Humana Press: Totowa, NJ, 2011; Vol. *681*, pp 485−496.

(9) Arnold, T.; Linke, D. The Use of Detergents to Purify Membrane Proteins. In *Current Protocols in Protein Science*; Coligan, J. E., Dunn, B. M., Speicher, D. W., Wingfield, P. T., Eds.; John Wiley & Sons, Inc.: Hoboken, NJ, 2008; p 4.8.1−4.8.30.

(10) Privé, G. G. Lipopeptide Detergents for Membrane Protein Studies. *Curr. Opin. Struct. Biol.* **2009**, *19* (4), 379−385.

(11) Baylon, J. L.; Vermaas, J. V.; Muller, M. P.; Arcario, M. J.; Pogorelov, T. V.; Tajkhorshid, E. Atomic-Level Description of Protein−lipid Interactions Using an Accelerated Membrane Model. *Biochim. Biophys. Acta, Biomembr.* **2016**, *1858* (7), 1573−1583.

(12) Hedger, G.; Sansom, M. S. P. Lipid Interaction Sites on Channels, Transporters and Receptors: Recent Insights from Molecular Dynamics Simulations. *Biochim. Biophys. Acta, Biomembr.* **2016**, *1858* (10), 2390−2400.

(13) Parmar, M. J.; Lousa, C. D. M.; Muench, S. P.; Goldman, A.; Postis, V. L. G. Artificial Membranes for Membrane Protein Purification, Functionality and Structure Studies. *Biochem. Soc. Trans.* **2016**, *44* (3), 877−882.

(14) Bayburt, T. H.; Grinkova, Y. V.; Sligar, S. G. Self-Assembly of Discoidal Phospholipid Bilayer Nanoparticles with Membrane Scaffold Proteins. *Nano Lett.* **2002**, *2* (8), 853−856.

(15) Bayburt, T. H.; Sligar, S. G. Membrane Protein Assembly into Nanodiscs. *FEBS Lett.* **2010**, *584* (9), 1721−1727.

(16) Skar-Gislinge, N.; Arleth, L. Small-Angle Scattering from Phospholipid Nanodiscs: Derivation and Refinement of a Molecular Constrained Analytical Model Form Factor. *Phys. Chem. Chem. Phys.* **2011**, *13* (8), 3161−3170.

(17) Skar-Gislinge, N.; Kynde, S. A. R.; Denisov, I. G.; Ye, X.; Lenov, I.; Sligar, S. G.; Arleth, L. Small-Angle Scattering Determination of the Shape and Localization of Human Cytochrome P450 Embedded in a Phospholipid Nanodisc Environment. *Acta Crystallogr., Sect. D: Biol. Crystallogr.* **2015**, *71* (12), 2412−2421.

(18) Pandit, A.; Shirzad-Wasei, N.; Wlodarczyk, L. M.; van Roon, H.; Boekema, E. J.; Dekker, J. P.; de Grip, W. J. Assembly of the Major Light-Harvesting Complex II in Lipid Nanodiscs. *Biophys. J.* **2011**, *101* (10), 2507−2515.

(19) Frauenfeld, J.; Gumbart, J.; van der Sluis, E. O.; Funes, S.; Gartmann, M.; Beatrix, B.; Mielke, T.; Berninghausen, O.; Becker, T.; Schulten, K.; Beckmann, R. Cryo-EM Structure of the Ribosome−SecYE Complex in the Membrane Environment. *Nat. Struct. Mol. Biol.* **2011**, *18* (5), 614−621.

(20) Wang, X.; Mu, Z.; Li, Y.; Bi, Y.; Wang, Y. Smaller Nanodiscs Are Suitable for Studying Protein Lipid Interactions by Solution NMR. *Protein J.* **2015**, *34* (3), 205−211.

(21) Mörs, K.; Roos, C.; Scholz, F.; Wachtveitl, J.; Dötsch, V.; Bernhard, F.; Glaubitz, C. Modified Lipid and Protein Dynamics in Nanodiscs. *Biochim. Biophys. Acta, Biomembr.* **2013**, *1828* (4), 1222−1229.

(22) Nikolaev, M.; Round, E.; Gushchin, I.; Polovinkin, V.; Balandin, T.; Kuzmichev, P.; Shevchenko, V.; Borshchevskiy, V.; Kuklin, A.; Round, A.; Bernhard, F.; Willbold, D.; Büldt, G.; Gordeliy, V. Integral Membrane Proteins Can Be Crystallized Directly from Nanodiscs. *Cryst. Growth Des.* **2017**, *17* (3), 945−948.

(23) Jamshad, M.; Grimard, V.; Idini, I.; Knowles, T. J.; Dowle, M. R.; Schofield, N.; Sridhar, P.; Lin, Y.; Finka, R.; Wheatley, M.; Thomas, O. R. T.; Palmer, R. E.; Overduin, M.; Govaerts, C.; Ruysschaert, J.-M.; Edler, K. J.; Dafforn, T. R. Structural Analysis of a Nanoparticle Containing a Lipid Bilayer Used for Detergent-Free Extraction of Membrane Proteins. *Nano Res.* **2015**, *8* (3), 774−789.

(24) Lee, S. C.; Knowles, T. J.; Postis, V. L. G.; Jamshad, M.; Parslow, R. A.; Lin, Y.; Goldman, A.; Sridhar, P.; Overduin, M.; Muench, S. P.; Dafforn, T. R. A Method for Detergent-Free Isolation of Membrane Proteins in Their Local Lipid Environment. *Nat. Protoc.* **2016**, *11* (7), 1149−1162.

(25) Routledge, S. J.; Mikaliunaite, L.; Patel, A.; Clare, M.; Cartwright, S. P.; Bawa, Z.; Wilks, M. D. B.; Low, F.; Hardy, D.; Rothnie, A. J.; Bill, R. M. The Synthesis of Recombinant Membrane Proteins in Yeast for Structural Studies. *Methods* **2016**, *95*, 26−37.

(26) Jamshad, M.; Charlton, J.; Lin, Y.; Routledge, S. J.; Bawa, Z.; Knowles, T. J.; Overduin, M.; Dekker, N.; Dafforn, T. R.; Bill, R. M.; Poyner, D. R.; Wheatley, M. G-Protein Coupled Receptor Solubilization and Purification for Biophysical Analysis and Functional Studies, in the Total Absence of Detergent. *Biosci. Rep.* **2015**, *35* (2), 1−10.

(27) Paulin, S.; Jamshad, M.; Dafforn, T. R.; Garcia-Lara, J.; Foster, S. J.; Galley, N. F.; Roper, D. I.; Rosado, H.; Taylor, P. W. Surfactant-Free Purification of Membrane Protein Complexes from Bacteria: Application to the Staphylococcal Penicillin-Binding Protein Complex PBP2/PBP2a. *Nanotechnology* **2014**, *25* (28), 285101.

(28) Gulati, S.; Jamshad, M.; Knowles, T. J.; Morrison, K. A.; Downing, R.; Cant, N.; Collins, R.; Koenderink, J. B.; Ford, R. C.; Overduin, M.; Kerr, I. D.; Dafforn, T. R.; Rothnie, A. J. Detergent-Free Purification of ABC (ATP-Binding-Cassette) Transporters. *Biochem. J.* **2014**, *461* (2), 269−278.

(29) Jamshad, M.; Lin, Y.-P.; Knowles, T. J.; Parslow, R. A.; Harris, C.; Wheatley, M.; Poyner, D. R.; Bill, R. M.; Thomas, O. R. T.; Overduin, M.; Dafforn, T. R. Surfactant-Free Purification of Membrane Proteins with Intact Native Membrane Environment. *Biochem. Soc. Trans.* **2011**, *39* (3), 813−818.

DOI: 10.1021/acs.biomac.7b01539
Biomacromolecules 2018, 19, 761−772

(30) Long, A. R.; O'Brien, C. C.; Malhotra, K.; Schwall, C. T.; Albert, A. D.; Watts, A.; Alder, N. N. A Detergent-Free Strategy for the Reconstitution of Active Enzyme Complexes from Native Biological Membranes into Nanoscale Discs. *BMC Biotechnol.* **2013**, *13* (1), 41.
(31) Prabudiansyah, I.; Kusters, I.; Caforio, A.; Driessen, A. J. M. Characterization of the Annular Lipid Shell of the Sec Translocon. *Biochim. Biophys. Acta, Biomembr.* **2015**, *1848* (10), 2050−2056.
(32) Postis, V.; Rawson, S.; Mitchell, J. K.; Lee, S. C.; Parslow, R. A.; Dafforn, T. R.; Baldwin, S. A.; Muench, S. P. The Use of SMALPs as a Novel Membrane Protein Scaffold for Structure Study by Negative Stain Electron Microscopy. *Biochim. Biophys. Acta, Biomembr.* **2015**, *1848* (2), 496−501.
(33) Bersch, B.; Dörr, J. M.; Hessel, A.; Killian, J. A.; Schanda, P. Proton-Detected Solid-State NMR Spectroscopy of a Zinc Diffusion Facilitator Protein in Native Nanodiscs. *Angew. Chem., Int. Ed.* **2017**, *56* (9), 2508−2512.
(34) Broecker, J.; Eger, B. T.; Ernst, O. P. Crystallogenesis of Membrane Proteins Mediated by Polymer-Bounded Lipid Nanodiscs. *Structure* **2017**, *25* (2), 384−392.
(35) Jamshad, M.; Grimard, V.; Idini, I.; Knowles, T.; Dowle, M.; Schofield, N.; Sridhar, P.; Lin, Y.; Finka, R.; Wheatley, M.; Thomas, O. T.; Palmer, R.; Overduin, M.; Govaerts, C.; Ruysschaert, J.-M.; Edler, K.; Dafforn, T. Structural Analysis of a Nanoparticle Containing a Lipid Bilayer Used for Detergent-Free Extraction of Membrane Proteins. *Nano Res.* **2014**, 774−789.
(36) Vargas, C.; Arenas, R. C.; Frotscher, E.; Keller, S. Nanoparticle Self-Assembly in Mixtures of Phospholipids with Styrene/Maleic Acid Copolymers or Fluorinated Surfactants. *Nanoscale* **2015**, *7* (48), 20685−20696.
(37) Helenius, A.; Simons, K. Solubilization of Membranes by Detergents. *Biochim. Biophys. Acta, Rev. Biomembr.* **1975**, *415* (1), 29−79.
(38) Heerklotz, H. Interactions of Surfactants with Lipid Membranes. *Q. Rev. Biophys.* **2008**, *41* (3−4), 205.
(39) Knowles, T. J.; Finka, R.; Smith, C.; Lin, Y.-P.; Dafforn, T.; Overduin, M. Membrane Proteins Solubilized Intact in Lipid Containing Nanoparticles Bounded by Styrene Maleic Acid Copolymer. *J. Am. Chem. Soc.* **2009**, *131* (22), 7484−7485.
(40) Orwick, M. C.; Judge, P. J.; Procek, J.; Lindholm, L.; Graziadei, A.; Engel, A.; Gröbner, G.; Watts, A. Detergent-Free Formation and Physicochemical Characterization of Nanosized Lipid−Polymer Complexes: Lipodisq. *Angew. Chem., Int. Ed.* **2012**, *51* (19), 4653−4657.
(41) Craig, A. F.; Clark, E. E.; Sahu, I. D.; Zhang, R.; Frantz, N. D.; Al-Abdul-Wahid, M. S.; Dabney-Smith, C.; Konkolewicz, D.; Lorigan, G. A. Tuning the Size of Styrene-Maleic Acid Copolymer-Lipid Nanoparticles (SMALPs) Using RAFT Polymerization for Biophysical Studies. *Biochim. Biophys. Acta, Biomembr.* **2016**, *1858* (11), 2931−2939.
(42) Lindhoud, S.; Carvalho, V.; Pronk, J. W.; Aubin-Tam, M.-E. SMA-SH: Modified Styrene-Maleic Acid Copolymer for Functionalization of Lipid Nanodiscs. *Biomacromolecules* **2016**, *17* (4), 1516−1522.
(43) Morrison, K. A.; Akram, A.; Mathews, A.; Khan, Z. A.; Patel, J. H.; Zhou, C.; Hardy, D. J.; Moore-Kelly, C.; Patel, R.; Odiba, V.; Knowles, T. J.; Javed, M. -u.-H.; Chmel, N. P.; Dafforn, T. R.; Rothnie, A. J. Membrane Protein Extraction and Purification Using Styrene-Maleic Acid (SMA) Copolymer: Effect of Variations in Polymer Structure. *Biochem. J.* **2016**, *473* (23), 4349−4360.
(44) Grethen, A.; Oluwole, A. O.; Danielczak, B.; Vargas, C.; Keller, S. Thermodynamics of Nanodisc Formation Mediated by Styrene/Maleic Acid (2:1) Copolymer. *Sci. Rep.* **2017**, *7* (1), 11517.
(45) Scheidelaar, S.; Koorengevel, M. C.; van Walree, C. A.; Dominguez, J. J.; Dörr, J. M.; Killian, J. A. Effect of Polymer Composition and PH on Membrane Solubilization by Styrene-Maleic Acid Copolymers. *Biophys. J.* **2016**, *111* (9), 1974−1986.
(46) Dominguez Pardo, J. J.; Dörr, J. M.; Renne, M. F.; Ould-Braham, T.; Koorengevel, M. C.; van Steenbergen, M.; Killian, J. A. Thermotropic Properties of Phosphatidylcholine Nanodiscs Bounded by Styrene-Maleic Acid Copolymers. *Chem. Phys. Lipids* **2017**, *208*, 58−64.
(47) Smith, A. A. A.; Autzen, H. E.; Laursen, T.; Wu, V.; Yen, M.; Hall, A.; Hansen, S. D.; Cheng, Y.; Xu, T. Controlling Styrene Maleic Acid Lipid Particles through RAFT. *Biomacromolecules* **2017**, *18* (11), 3706−2713.
(48) Harrisson, S.; Wooley, K. L. Shell-Crosslinked Nanostructures from Amphiphilic AB and ABA Block Copolymers of Styrene-Alt-(Maleic Anhydride) and Styrene: Polymerization, Assembly and Stabilization in One Pot. *Chem. Commun.* **2005**, *26*, 3259−3261.
(49) Kemmer, G.; Keller, S. Nonlinear Least-Squares Data Fitting in Excel Spreadsheets. *Nat. Protoc.* **2010**, *5* (2), 267−281.
(50) Cuevas Arenas, R.; Klingler, J.; Vargas, C.; Keller, S. Influence of Lipid Bilayer Properties on Nanodisc Formation Mediated by Styrene/Maleic Acid Copolymers. *Nanoscale* **2016**, *8* (32), 15016−15026.
(51) Hazell, G.; Arnold, T.; Barker, R. D.; Clifton, L. A.; Steinke, N.-J.; Tognoloni, C.; Edler, K. J. Evidence of Lipid Exchange in Styrene Maleic Acid Lipid Particle (SMALP) Nanodisc Systems. *Langmuir* **2016**, *32* (45), 11845−11853.
(52) Cuevas Arenas, R.; Danielczak, B.; Martel, A.; Porcar, L.; Breyton, C.; Ebel, C.; Keller, S. Fast Collisional Lipid Transfer Among Polymer-Bounded Nanodiscs. *Sci. Rep.* **2017**, *7*, 45875.
(53) Brewer, A. K.; Striegel, A. M. Characterizing the Size, Shape, and Compactness of a Polydisperse Prolate Ellipsoidal Particle via Quadruple-Detector Hydrodynamic Chromatography. *Analyst* **2011**, *136* (3), 515−519.
(54) Heimburg, T. A Model for the Lipid Pretransition: Coupling of Ripple Formation with the Chain-Melting Transition. *Biophys. J.* **2000**, *78* (3), 1154−1165.
(55) Blume, A. Apparent Molar Heat Capacities of Phospholipids in Aqueous Dispersion. Effects of Chain Length and Head Group Structure. *Biochemistry* **1983**, *22* (23), 5436−5442.
(56) Keddie, D. J.; Moad, G.; Rizzardo, E.; Thang, S. H. RAFT Agent Design and Synthesis. *Macromolecules* **2012**, *45* (13), 5321−5342.

DOI: 10.1021/acs.biomac.7b01539
Biomacromolecules 2018, 19, 761−772